Inorganic Chemistry
Article

Inorg. Chem. **2009**, *48*, 10737–10747 **10737**
DOI: 10.1021/ic901671j

$[Os^{IV}Cl_5(Hazole)]^-$ Complexes: Synthesis, Structure, Spectroscopic Properties, and Antiproliferative Activity

Gabriel E. Büchel, Iryna N. Stepanenko, Michaela Hejl, Michael A. Jakupec, Vladimir B. Arion,* and Bernhard K. Keppler

University of Vienna, Institute of Inorganic Chemistry, Währinger Strasse 42, A-1090 Vienna, Austria

Received August 21, 2009

By exploring the Anderson type rearrangement reactions, osmium(IV) complexes of the general formula $[cation]^+[Os^{IV}Cl_5(Hazole)]^-$, where $[cation]^+ = n\text{-}Bu_4N^+$, Hazole = 1*H*-pyrazole (Hpz) (**1**), 1*H*-indazole (Hind) (**2**), 1*H*-imidazole (Him) (**3**), 1*H*-benzimidazole (Hbzim) (**4**), 1*H*,2,4-triazole (Htrz) (**5**), have been synthesized. To improve water solubility of tetrabutylammonium compounds, complexes with $[cation]^+ = Na^+$ [Hazole = Hpz **6**), Hind (**7**), Htrz (**8**)] or H_2azole^+ [Hazole = Hpz (**9**), Hind (**10**), Htrz (**11**)] have been also prepared with the aim of testing them for cytotoxicity in cancer cells. In addition, the preparation of the complex $\{(n\text{-}Bu_4N)_2[Os^{IV}Cl_6]\}_2[Os^{IV}Cl_4(Him)_2]$ (**12**) is also reported. The compounds have been comprehensively characterized by elemental analysis, electrospray ionization (ESI) mass spectrometry, spectroscopy (IR, UV−vis, 1D and 2D NMR), cyclic voltammetry, X-ray crystallography (**1**−**6** and **12**) and magnetic susceptibility (**5**). Complexes **6**, **7**, **9** are kinetically inert in aqueous solution and resistant to hydrolysis. Compounds **6**−**11** were found to possess modest antiproliferative acitivity in vitro against CH1 (ovarian carcinoma), A549 (non−small cell lung carcinoma), and SW480 (colon adenocarcinoma) cells with IC_{50} values in the 10^{-4} M concentration range. Replacement of azolium cations by sodium had significant effects; cytotoxicity increased in the case of the pyrazole system from 3 (A549) to the 5.5−fold (CH1).

Introduction

The past several years have seen conscious efforts directed at the synthesis and screening of osmium coordination compounds and organometallic species as potential antitumor drugs,[1−3] as well as studies of their reactivity with DNA model compounds.[4]

The spectrum of the antiproliferative activity of osmium-based compounds reported so far is broadly varying from non-cytotoxic with IC_{50} values exceeding 1600 μM (e.g., $[Os(\eta^6\text{-}p\text{-cymene})(pta)Cl_2]$,[1b] where pta = 1,3,5-triaza-7-phosphatricyclo[3.3.1.1]decane (in the human T47D breast carcinoma cell line), to fairly cytotoxic with IC_{50} values in the low micromolar concentration range from 1 to 10 μM, comparable to that of carboplatin, as in the case of $[Os(\eta^6\text{-biphenyl})(dppz)Cl]PF_6$,[2c] where dppz = [3,2-a: 2′,3′-*c*]phenazine (in the human A2780 ovarian carcinoma cell line), $[Os(\eta^6\text{-biphenyl})(pico)Cl]$,[2d] where pico = picolinate (in the human A549 non-small cell lung cancer and A2780), $[Os(\eta^6\text{-p-cymene})(oxine)(Hazole)]Cl$,[3e] where oxine = deprotonated 8-hydroxyquinoline, and Hazole = azole heterocycle, i.e., pyrazole, imidazole (in the human CH1 ovarian carcinoma and SW480 colon carcinoma cell lines), $[Os(\eta^6\text{-p-cymene})(paullone)Cl]Cl$,[3c,d] (in CH1, SW480 and A549), *trans*-$[Os^{III}Cl_2(Hazole)_4]Cl$,[3b] where Hazole = pyrazole, benzimidazole (in A549, CH1 and SW480 cells).

*To whom correspondence should be addressed. E-mail: vladimir.arion@univie.ac.at. Phone: +431427752615. Fax: +431427752680.

(1) (a) Allardyce, C. S.; Dorcier, A.; Scolaro, C.; Dyson, P. J. *Appl. Organomet. Chem.* **2005**, *19*, 1–10. (b) Dorcier, A.; Ang, W. H.; Bolaño, S.; Gonsalvi, L.; Juillerat-Jeannerat, L.; Laurenczy, G.; Peruzzini, M.; Phillips, A. D.; Zanobini, F.; Dyson, P. J. *Organometallics* **2006**, *25*, 4090–4096. (c) Dyson, P. J. *Chimia* **2007**, *61*, 698–703. (d) Renfrew, A. K.; Phillips, A. D.; Egger, A. E.; Hartinger, C. G.; Bosquain, S. S.; Nazarov, A. A.; Keppler, B. K.; Gonsalvi, L.; Peruzzini, M.; Dyson, P. J. *Organometallics* **2009**, *28*, 1165–1172.

(2) (a) Peacock, A. F. A.; Habtemariam, A.; Fernandez, R.; Walland, V.; Fabbiani, F. P. A.; Parsons, S.; Aird, R. E.; Jodrell, D. I.; Sadler, P. J. *J. Am. Chem. Soc.* **2006**, *128*, 1739–1748. (b) Peacock, A. F. A.; Melchart, M.; Deeth, R. J.; Habtemariam, A.; Parsons, S.; Sadler, P. J. *Chem. Eur. J.* **2007**, *13*, 2601–2613. (c) Peacock, A. F. A.; Habtemariam, A.; Moggach, S. A.; Prescimone, A.; Parsons, S.; Sadler, P. J. *Inorg. Chem.* **2007**, *46*, 4049–4059. (d) Peacock, A. F. A.; Parsons, S.; Sadler, P. J. *J. Am. Chem. Soc.* **2007**, *129*, 3348–3357. (e) van Rijt, S. H.; Peacock, A. F. A.; Johnstone, R. D. L.; Parsons, S.; Sadler, P. J. *Inorg. Chem.* **2009**, *48*, 1753–1752.

(3) (a) Cebrián-Losantos, B.; Krokhin, A. A.; Stepanenko, I. N.; Eichinger, R.; Jakupec, M. A.; Arion, V. B.; Keppler, B. K. *Inorg. Chem.* **2007**, *46*, 5023–5033. (b) Stepanenko, I. N.; Krokhin, A. A.; John, R. O.; Roller, A.; Arion, V. B.; Jakupec, M. A.; Keppler, B. K. *Inorg. Chem.* **2008**, *47*, 7338–7347. (c) Schmid, W. F.; John, R. O.; Arion, V. B.; Jakupec, M. A.; Keppler, B. K. *Organometallics* **2007**, *26*, 6643–6652. (d) Schmid, W. F.; John, R. O.; Mühlgassner, G.; Heffeter, P.; Jakupec, M. A.; Galanski, M.; Berger, W.; Arion, V. B.; Keppler, B. K. *J. Med. Chem.* **2007**, *50*, 6343–6355. (e) Schuecker, R.; John, R. O.; Jakupec, M. A.; Arion, V. B.; Keppler, B. K. *Organometallics* **2008**, *27*, 6587–6595.

(4) (a) Dorcier, A.; Dyson, P. J.; Gossens, C.; Rothlisberger, U.; Scopelliti, R.; Tavernelli, I. *Organometallics* **2005**, *24*, 2114–2123. (b) Dorcier, A.; Hartinger, C. J.; Scopelliti, R.; Fish, R. H.; Keppler, B. K.; Dyson, P. J. *J. Inorg. Biochem.* **2008**, *102*, 1066–1076.

Published on Web 10/20/2009

Comparison of antiproliferative activity of closely related ruthenium and osmium compounds shows that these can be very similar, as is the case for [Ru(η^6-biphenyl)(en)Cl]BPh_4 and [Os(η^6-biphenyl)(en)Cl]BF_4,[2b,c] similar against certain human cancer cell lines, while different in respect to other cells,[1b,3b] or quite contrasting, as is the case for compounds closely related to $(H_2im)[Ru^{III}Cl_4(DMSO)(Him)]$ (NAMI-A), an antimetastatic drug candidate which just entered phase II clinical trials.[5] The IC_{50} value for $(H_2ind)[Os^{III}Cl_4(DMSO)(Hind)]$ in the human cancer cell line HT29 (colon carcinoma) is $21 \pm 1\ \mu M$. This is 1 order of magnitude lower than the respective value for its ruthenium congener ($212 \pm 22\ \mu M$).[3a] Reversed activity profiles were documented for *trans*-$[Os^{III}Cl_2(Him)_4]Cl$ and its ruthenium analogue.[3b]

Investigation of osmium compounds is of particular interest not only because it complements the growing family of ruthenium compounds which exhibit antitumor activity but also because of well established differences between the metals, reflected in preparation approaches to their coordination and organometallic compounds, the preference for higher oxidation states, the stronger π back-donation from lower oxidation states, and the much stronger spin−orbit coupling of the heavier congener, as well as the marked differences in metal−ligand exchange kinetics, which are essential for their medicinal applicability as anticancer drugs.[6−8] The advantage of using osmium analogues with a cytotoxicity similar to their ruthenium congener lies in their higher inertness under conditions relevant for drug formulation.[2c] All this suggests that osmium is another metal that deserves attention for the development of effective inorganic antitumor drugs.

Being involved in the development of metal-based antitumor drugs, compounds of the general formula $[Ru^{III}Cl_{(6-n)}(Hazole)_n]^{(3-n)-}$, with $n = 1-4$, were prepared and tested for antiproliferative activity in human cancer cell lines. A correlation between cytotoxicity in the two cell lines and Ru^{III}/Ru^{II} redox potentials was found.[9] The antiproliferative activity of these compounds varied broadly in the following order: $[Ru^{III}Cl_6]^{3-} < [Ru^{III}Cl_4(Hind)_2]^- < [Ru^{III}Cl_5(Hind)]^{2-} \ll [Ru^{III}Cl_3(Hind)_3] < [Ru^{III}Cl_2(Hind)_4]^+$,[9] but largely correlated with their redox potentials.

In pursuing the long-term goal of establishing structure−cytotoxicity relationships for the osmium-azole-chlorido series, we already reported the synthesis of *trans*-$[Os^{III}Cl_2(Hazole)_4]Cl$, *cis*-$[Os^{III}Cl_2(Him)_4]Cl$, and *mer*-$[Os^{III}Cl_3(Hazole)_3]$.[3b,10,11] Compounds of the last type were insoluble in water, precluding their testing for antiproliferative activity in vitro. Herein we report the synthesis and characterization of the first members of a new series, namely, complexes of the general formula $[cation]^+[Os^{IV}Cl_5(Hazole)]^-$, where $[cation]^+ = n\text{-}Bu_4N^+$ [Hazole = 1*H*-pyrazole (Hpz) (**1**), 1*H*-indazole (Hind) (**2**), 1*H*-imidazole (Him) (**3**), 1*H*-benzimidazole (Hbzim) (**4**), 1*H*,2,4-triazole (Htrz) (**5**)], Na^+ [Hazole = Hpz (**6**), Hind (**7**), Htrz (**8**)] or H_2azole^+ [Hazole = Hpz (**9**), Hind (**10**), Htrz (**11**)] (Chart 1). The antiproliferative activity of compounds **6**−**11** in three human cancer cell lines was assessed and compared to that of ruthenium(III) analogues $(H_2azole)_2[Ru^{III}Cl_5(Hazole)]$.[12] In addition, the synthesis and crystal structure of the complex $\{(Bu_4N)_2[Os^{IV}Cl_6]\}_2[Os^{IV}Cl_4(Him)_2]$ (**12**) is reported.

Chart 1. Compounds Reported in This Work[a]

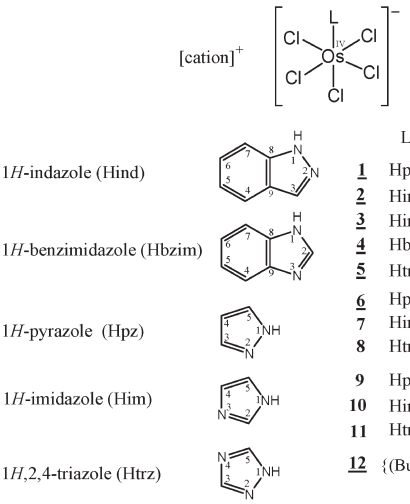

	L	[cation]+
1	Hpz	Bu_4N^+
2	Hind	Bu_4N^+
3	Him	Bu_4N^+
4	Hbzim	Bu_4N^+
5	Htrz	Bu_4N^+
6	Hpz	Na^+
7	Hind	Na^+
8	Htrz	Na^+
9	Hpz	H_2pz^+
10	Hind	H_2ind^+
11	Htrz	H_2trz^+
12	$\{(Bu_4N)_2[Os^{IV}Cl_6]\}_2.[Os^{IV}Cl_4(Him)_2]$	

n-Tetrabutylammonium $n\text{-}(Bu_4N)(CH_3{}^D\text{-}CH_2{}^C\text{-}CH_2{}^B\text{-}CH_2{}^A)_4N^+$

[a] Underlined complexes have been characterized by X-ray crystallography; atom labeling was introduced for assignments of resonances in NMR spectra.

Experimental Section

Materials. The starting compounds $[(DMSO)_2H]_2[OsCl_6]$ and $(H_2azole)_2[OsCl_6]$ (Hazole = Hpz, Him, Hind, Hbzim) were synthesized as previously reported in the literature.[13,14] OsO_4 (99.8%) and $N_2H_4 \cdot 2HCl$ were purchased from Johnson Matthey and Fluka, respectively. 1*H*-pyrazole, 1*H*-indazole, 1*H*-imidazole, and 1*H*-benzimidazole were from Aldrich and Fluka and 1*H*,2,4-triazole from Acros. All these chemicals were used without further purification. $(Bu_4N)[OsCl_5(Hazole)]$ complexes were prepared under argon atmosphere using standard Schlenk techniques as described below. Solvents were distilled according to standard procedures.[15]

(Bu_4N)[$OsCl_5$(Hpz)] (1). To a solution of $(H_2pz)_2[OsCl_6]$ (100 mg, 0.18 mmol) in dry ethanol (10 mL) excess Bu_4NCl (153 mg, 0.55 mmol) was added. The suspension was stirred at 85 °C for 24 h. The volume of the solvent was then reduced to a quarter, and the reaction mixture was allowed to stand at −20 °C for 2 days. The yellow product formed was filtered off and purified by column chromatography on silica, using as eluent a mixture of $CHCl_3/CH_3OH$ 4:1 and collecting the first fraction ($R_f = 0.75$). Yield: 30 mg, 24%. Anal. Calcd for $C_{19}H_{40}Cl_5N_3Os$

(5) Gianferrara, T.; Bratsos, I.; Alessio, E. *Dalton Trans.* **2009**, *37*, 7588–7598.
(6) Stepanenko, I. N.; Cebrián-Losantos, B.; Arion, V. B.; Krokhin, A. A.; Nazarov, A. A.; Keppler, B. K. *Eur. J. Inorg. Chem.* **2007**, 400–411.
(7) Singh, P.; Sarkar, B.; Sieger, M.; Niemeyer, M.; Fiedler, J.; Zališ, S.; Kaim, W. *Inorg. Chem.* **2006**, *45*, 4602–4609.
(8) Peacock, A. F. A.; Sadler, P. J. *Chem. Asian. J.* **2008**, *3*, 1890–1899.
(9) Jakupec, M. A.; Reisner, E.; Eichinger, A.; Pongratz, M.; Arion, V. B.; Galanski, M.; Hartinger, C. G.; Keppler, B. K. *J. Med. Chem.* **2005**, *48*, 2831–2837.
(10) Chiorescu, I.; Stepanenko, I. N.; Arion, V. B.; Krokhin, A. A.; Keppler, B. K. ICBIC XIII, **2007**, July 15−20, Vienna, Austria, *J. Biol. Inorg. Chem.* (**2007**) *12* (Suppl. 1): P456, S 226.
(11) Chiorescu, I.; Stepanenko, I. N.; Arion, V. B.; Krokhin, A. A.; Yulia Yu. Scaffidi-Domianello, Y. Y; Keppler, B. K. *EUROBIC 8*, **2006**, July 2−7, Aveiro, Portugal, PS7.17, p 333.
(12) Lipponer, K.-G.; Vogel, E.; Keppler, B. K. *Met.-Based Drugs* **1996**, *3*, 243–260.
(13) Brauer, G. *Handbuch der Präparativen Anorg. Chem., III* **1981**, 1742–1744.
(14) Rudnitskaya, O. V.; Buslaeva, T. M.; Lyalina, N. N. *Zh. Neorg. Khim.* **1994**, *39*, 922–924.
(15) Perrin, D. D.; Armarego, W. L. F. *Purification of Laboratory Chemicals*, 3rd ed.; Butterworth Heinemann: Oxford, 1988.

(M_r = 677.99 g/mol): C, 33.66; H, 5.95; N, 6.20. Found: C, 33.73; H, 5.73; N, 6.11. ESI-MS in MeOH (negative): *m*/*z* 435 $[Os^{IV}Cl_5(Hpz)]^-$, 367 $[Os^{IV}Cl_5]^-$. IR, cm^{-1}: 573, 665, 740, 773, 881, 1053, 1125, 1165, 1265, 1352, 1381, 1404, 1472, 1513, 2872, 2961, 3142, and 3330. UV−vis (C_2H_5OH), λ_{max}, nm (ε, M^{-1} cm^{-1}): 254 sh (4 064), 360 (9 503). ^1H NMR (d_6-DMSO, 500.32 MHz): δ −2.71 (s, 1H), −2.44 (s, 1H), 0.95 (t, $12H_D$, J = 7.4 Hz), 1.32 (sxt, $8H_C$, J = 7.4 Hz), 1.58 (qui, $8H_B$, J = 7.8 Hz), 3.17 (t, $8H_A$, J = 8.4 Hz), 6.39 (d, J = 1.6 Hz), 15.71 (s, $1H_1$) ppm. $^{13}C\{^1H\}$ NMR (d_6-DMSO, 125.81 MHz): δ 14.11 (C_D), 19.88 (C_C), 23.78 (C_B), 58.43 (C_A), 71.08 {6.39}, 180.92 {−2.71}, 191.31 {−2.44} ppm. ^{15}N NMR (d_6-DMSO, 50.68 MHz): δ 144.3 (N_1) ppm. Suitable crystals for X-ray diffraction study were selected directly from the reaction vessel.

(Bu_4N)[$OsCl_5$(Hind)] (2). To a solution of $(H_2ind)_2[OsCl_6]$ (100 mg, 0.16 mmol) in dry ethanol (15 mL) excess Bu_4NCl (150 mg, 0.54 mmol) was added. The suspension was stirred at 85 °C for 24 h. The volume of the solvent was then reduced to a quarter, and the reaction mixture was allowed to stand at room temperature overnight. The dark-red product formed was filtered off and purified by column chromatography on silica, using as eluent a mixture of $CHCl_3/CH_3OH$ 7:1 and collecting the first fraction (R_f = 0.67). Yield: 80 mg, 70%. Anal. Calcd for $C_{23}H_{42}Cl_5N_3Os$ (M_r = 728.05 g/mol): C, 37.94; H, 5.81; N, 5.77. Found: C, 38.05; H, 5.78; N, 5.66. ESI-MS in MeOH (negative): *m*/*z* 485 $[Os^{IV}Cl_5(Hind)]^-$, 332 $[Os^{III}Cl_4]^-$. IR, cm^{-1}: 431, 613, 752, 883, 1089, 1147, 1241, 1360, 1378, 1475, 1513, 1627, 2872, 2959, and 3341. UV−vis (C_2H_5OH), λ_{max}, nm (ε, M^{-1} cm^{-1}): 282 (9 492), 362 (11 031). ^1H NMR (d_6-DMSO, 500.32 MHz): δ −4.54 (s, $1H_3$), 0.95 (t, $12H_D$, J = 7.3 Hz), 1.32 (sxt, $8H_C$, J = 7.3 Hz), 1.58 (qui, $8H_B$, J = 7.8 Hz), 3.08 (t, $1H_6$, J = 7.7 Hz), 3.17 (t, $8H_A$, J = 8.4 Hz), 5.89 (d, $1H_4$, J = 8.2 Hz), 8.24 (t, $1H_5$, J = 7.5 Hz), 10.84 (d, $1H_7$, J = 8.5 Hz), 17.76 (s, $1H_1$) ppm. $^{13}C\{^1H\}$ NMR (d_6-DMSO, 125.81 MHz): δ 14.08 (C_D), 19.84 (C_C), 23.74 (C_B), 58.36 (C_A), 75.94 (C_9), 81.88 (C_7), 106.16 (C_5), 139.58 (C_4), 163.74 (C_6), 173.67 (C_8), 200.66 (C_3) ppm. ^{15}N NMR (d_6-DMSO, 50.68 MHz): δ 124.7 (N_1) ppm. X-ray diffraction quality single crystals were obtained by slow diffusion of hexane into a chloroform solution of **2** in a NMR tube.

(Bu_4N)[$OsCl_5$(Him)] (3). A mixture of $(H_2im)_2[OsCl_6]$ (12 mg, 0.02 mmol) and excess Bu_4NCl (16 mg, 0.06 mmol) in isoamyl alcohol (1 mL) was stirred at 100 °C for 72 h. The solvent was evaporated, and the red residue was dissolved in methanol. The mixture was allowed to stand at −20 °C for 2 days, producing single crystals suitable for X-ray diffraction study.

(Bu_4N)[$OsCl_5$(Hbzim)] (4). To a solution of $(H_2bzim)_2[OsCl_6]$ (100 mg, 0.16 mmol) in dry ethanol (15 mL) excess Bu_4NCl (130 mg, 0.47 mmol) was added. The suspension was stirred at 85 °C for 24 h. The volume of the solvent was then reduced to a quarter. The dark-red product formed was separated by filtration and purified by column chromatography on silica, using as eluent a mixture of $CHCl_3/CH_3OH$ 7:1 and collecting the second fraction (R_f = 0.47). Yield: 90 mg, 79%. Anal. Calcd for $C_{23}H_{42}Cl_5N_3Os$ (M_r = 728.09 g/mol): C, 37.94; H, 5.81; N, 5.77. Found: C, 37.84; H, 5.53; N, 5.59. ESI-MS in MeOH (negative): *m*/*z* 485 $[Os^{IV}Cl_5(Hbzim)]^-$, 450 $[Os^{III}Cl_4(Hbzim)]^-$, 367 $[Os^{IV}Cl_5]^-$, 332 $[Os^{III}Cl_4]^-$. IR, cm^{-1}: 613, 699, 737, 760, 798, 882, 981, 1012, 1106, 1150, 1184, 1243, 1265, 1303, 1379, 1411, 1477, 1504, 2873, 2931, 2962, 3269. UV−vis (C_2H_5OH), λ_{max}, nm (ε, M^{-1} cm^{-1}): 267 (10 253), 342 sh (7 109), 366 (9 034). ^1H NMR (d_6-DMSO, 500.32 MHz): δ −4.64 (s, $1H_2$), 0.94 (t, $12H_D$, J = 7.3 Hz), 1.32 (sxt, $8H_C$, J = 7.3 Hz), 1.58 (qui, $8H_B$, J = 7.6 Hz), 3.17 (t, $8H_A$, J = 8.4 Hz), 6.04 (t, $1H_{5\ or\ 6}$, J = 7.3 Hz), 6.52 (d, $1H_{4\ or\ 7}$, J = 8.2 Hz), 6.98 (t, $1H_{5\ or\ 6}$, J = 7.7 Hz), 7.34 (d, $1H_{4\ or\ 7}$, J = 8.1 Hz), 9.41 (s, $1H_1$) ppm. X-ray diffraction quality crystals of **4**·CH_3OH were obtained from a solution of **4** in methanol at −16 °C after 24 h.

(Bu_4N)[$OsCl_5$(Htrz)]·C_2H_5OH (5·C_2H_5OH). To a solution of $(H_2trz)_2[OsCl_6]$ (300 mg, 0.55 mmol) in dry ethanol (10 mL) excess Bu_4NCl (450 mg, 1.62 mmol) was added. The suspension was stirred at 85 °C for 24 h. The solution produced yellow needle-like crystals on cooling. These were filtered off, washed with diethyl ether (2 × 5 mL) and dried in vacuo. Yield: 130 mg, 33%. Anal. Calcd for $C_{18}H_{39}Cl_5N_4Os·C_2H_5OH$ (M_r = 725.05 g/mol): C, 33.13; H, 6.26; N, 7.73. Found: C, 33.28; H, 6.29; N, 7.81. ESI-MS in MeOH (negative): *m*/*z* 436 $[Os^{IV}Cl_5(Htrz)]^-$, 367 $[Os^{IV}Cl_5]^-$. IR, cm^{-1}: 584, 631, 736, 880, 1001, 1059, 1306, 1381, 1427, 1466, 1983, 2359, 2872, 2960. UV−vis (C_2H_5OH), λ_{max}, nm (ε, M^{-1} cm^{-1}): 270 sh (5 076), 366 (10 384), 425 sh (2 365). ^1H NMR (d_6-DMSO, 500.32 MHz): δ −2.22 (brs), 0.94 (t, $12H_D$, J = 7.3 Hz), 1.32 (sxt, $8H_C$, J = 7.3 Hz), 1.58 (qui, $8H_B$, J = 7.5 Hz), 3.17 (t, $8H_A$, J = 8.3 Hz), 9.39 (brs), 13.65 (brs) ppm. Suitable crystals of **5**·C_2H_5OH for X-ray diffraction study were selected directly from the reaction vessel.

Na[$OsCl_5$(Hpz)]·$2H_2O$ (6·$2H_2O$). To a solution of **1** (106 mg, 0.16 mmol) in water (400 mL) ion exchanger Dowex Marathon C Na^+−form (10 g), after 12 h of soaking in water, was added. The suspension was stirred for 30 min, the ion exchanger separated by filtration, and the solution lyophilized, to give a brown solid. Yield: 73 mg, 94%. Anal. Calcd for $C_3H_4Cl_5N_2NaOs·2H_2O$ (M_r = 494.55 g/mol): C, 7.29; H, 1.63; N, 5.66. Found: C, 7.77; H, 1.35; N, 5.23. ESI-MS in MeOH (negative): *m*/*z* 400 $[Os^{III}Cl_4(Hpz)]^-$, 367 $[Os^{IV}Cl_5]^-$. Solubility in water 34.3 mM at 298 K. IR, cm^{-1}: 569, 656, 768, 905, 1055, 1072, 1111, 1169, 1265, 1345, 1398, 1485, 1506, 1620, 3144, 3314, 3481, 3559. UV−vis (H_2O), λ_{max}, nm (ε, M^{-1} cm^{-1}): 207 (15 376), 256 sh (3 663), 351 (6 131), 368 sh (6 079). ^1H NMR (d_6-DMSO, 500.32 MHz): δ −2.75 (s, 1H), −2.48 (s, 1H), 6.34 (s, 1H), 15.69 (s, $1H_1$) ppm. X-ray diffraction quality crystals were obtained by slow evaporation of a solution of **6** in water.

Na[$OsCl_5$(Hind)]·$2H_2O$ (7·$2H_2O$). To a solution of **2** (50 mg, 0.07 mmol) in water/ethanol 1:1 (160 mL) ion exchanger Dowex Marathon C Na^+−form (5 g), after 12 h of soaking in water, was added. The suspension was stirred for 30 min, the ion exchanger separated by filtration, and the solution lyophilized, to give a brown solid. Yield: 34 mg, 91%. Anal. Calcd for $C_7H_6Cl_5N_2NaOs·2H_2O$ (M_r = 544.65 g/mol): C, 15.44; H, 1.85; N, 5.14. Found: C, 15.64; H, 1.64; N, 5.03. ESI-MS in MeOH/CH_3CN (negative): *m*/*z* 485 $[Os^{IV}Cl_5(Hind)]^-$, 367 $[Os^{IV}Cl_5]^-$. Solubility in water 3.9 mM at 298 K. IR, cm^{-1}: 636, 748, 759, 785, 967, 1087, 1243, 1360, 1516, 1626, 3307, 3355, 3471, 3551. UV−vis (H_2O), λ_{max}, nm (ε, M^{-1} cm^{-1}): 199 (760 730), 269 (159 591), 359 (143 943), 403 sh (96406). ^1H NMR (d_6-DMSO, 500.32 MHz): δ −4.54 (s, $1H_3$), 3.08 (t, $1H_6$, J = 7.7 Hz), 5.89 (d, $1H_4$, J = 8.2 Hz), 8.24 (t, $1H_5$, J = 7.6 Hz), 10.84 (d, $1H_7$, J = 8.5 Hz), 17.76 (s, $1H_1$) ppm.

Na[$OsCl_5$(Htrz)]·$1.5H_2O$ (8·$1.5H_2O$). To a solution of **5** (100 mg, 0.15 mmol) in water (420 mL) ion exchanger Dowex Marathon C Na^+−form (10 g), after 12 h of soaking in water, was added. The suspension was allowed to stir for 30 min, the ion exchanger separated by filtration, and the solution lyophilized, to give an orange solid. Yield: 70 mg, 98%. Anal. Calcd for $C_2H_3Cl_5N_3NaOs·1.5H_2O$ (M_r = 486.57 g/mol): C, 4.94; H, 1.24; N, 8.64. Found: C, 5.24; H, 1.08; N, 8.28. ESI-MS in MeOH (negative): *m*/*z* 436 $[Os^{IV}Cl_5(Htrz)]^-$, 401 $[Os^{III}Cl_4(Htrz)]^-$, 367 $[Os^{IV}Cl_5]^-$, 332 $[Os^{III}Cl_4]^-$. Solubility in water 15.4 mM at 298 K. IR, cm^{-1}: 573, 614, 676, 865, 890, 962, 1079, 1144, 1192, 1257, 1301, 1374, 1412, 1493, 1523, 1613, 2363, 3127, 3322, 3534. UV−vis (H_2O), λ_{max}, nm (ε, M^{-1} cm^{-1}): 343 sh (5 432), 362 (6 112). ^1H NMR (d_6-DMSO, 500.32 MHz): δ −7.23 (brs) ppm.

(H_2pz)[$OsCl_5$(Hpz)]·H_2O (9·H_2O). To pyrazole (14 mg, 0.21 mmol) in water (1.4 mL) 12 M hydrochloric acid (0.02 mL, 0.24 mmol) was added. The resulting solution of pyrazolium chloride was then added to a solution of **6** (47 mg, 0.10 mmol) in water (0.6 mL). The reaction mixture produced red crystals. Yield: 26 mg, 52%. Anal. Calcd for $C_6H_9Cl_5N_4Os·H_2O$ (M_r = 522.67): C, 13.79; H, 2.12; N, 10.72. Found: C, 13.82; H, 1.82; N, 10.32.

ESI-MS in MeOH (negative): m/z 435 $[Os^{IV}Cl_5(Hpz)]^-$, 367 $[Os^{IV}Cl_5]^-$, 332 $[Os^{III}Cl_4]^-$. Solubility in water 6.7 mM at 298 K. IR, cm^{-1}: 599, 609, 771, 905, 1051, 1070, 1110, 1131, 1170, 1276, 1351, 1398, 1487, 1524, 1563, 1601, 2862, 3044, 3136, 3472, 3513. UV−vis (H_2O), λ_{max}, nm (ε, M^{-1} cm^{-1}): 208 (19 463), 253 sh (3 806), 357 (8 678). ^1H NMR (d_6-DMSO, 500.32 MHz): δ −2.71 (s, 1H), −2.44 (s, 1H), 6.31 (s, $1H_4'$), 6.39 (s, 1H), 7.68 (s, $2H_{3,5}'$), 15.71 (s, $1H_1$) ppm. $^{13}C\{^1H\}$ NMR (d_6-DMSO, 125.81 MHz): δ 71.18 {6.39}, 106.16 (C_4'), 134.25 ($C_{3,5}'$), 181.33 {−2.71}, 191.99 {−2.44} ppm. ^{15}N NMR (d_6-DMSO, 50.68 MHz): δ 144.1 (N_1) ppm.

(H_2ind)[$OsCl_5$(Hind)]·H_2O (10·H_2O). To indazole (12 mg, 0.10 mmol) in water (1.2 mL) was added 12 M hydrochloric acid (0.01 mL, 0.12 mmol). The resulting solution of indazolium chloride was then added to a solution of **7** (45 mg, 0.08 mmol) in water (4 mL). The reaction mixture produced a brown solid. Yield: 40 mg, 78%. Anal. Calcd for $C_{14}H_{13}Cl_5N_4Os \cdot H_2O$ (M_r = 622.79): C, 27.00; H, 2.43; N, 9.00. Found: C, 27.36; H, 2.31; N, 8.72. ESI-MS in $MeOH/CH_3CN$ (negative): m/z 485 $[Os^{IV}Cl_5(Hind)]^-$, 367 $[Os^{IV}Cl_5]^-$. Solubility in water 1.3 mM at 298 K. IR, cm^{-1}: 614, 744, 787, 830, 967, 1002, 1087, 1126, 1152, 1247, 1359, 1384, 1483, 1516, 1628, 2359, 3127, 3248, 3466, 3519. UV−vis (H_2O), λ_{max}, nm (ε, M^{-1} cm^{-1}): 201 (31 605), 249 (4 565), 286 (4 721), 358 (3 571). ^1H NMR (d_6-DMSO, 500.32 MHz): δ −4.56 (s, $1H_3$), 3.06 (t, $1H_6$, J = 7.7 Hz), 5.89 (d, $1H_4$, J = 7.5 Hz), 7.11 (t, $1H_5'$, J = 7.4 Hz), 7.34 (t, $1H_6'$, J = 7.6 Hz), 7.53 (d, $1H_7'$, J = 8.4 Hz), 7.75 (d, $1H_4'$, J = 8.1 Hz), 8.08 (s, $1H_3'$), 8.23 (t, $1H_5$, J = 7.6 Hz), 10.85 (d, $1H_7$, J = 8.5 Hz), 17.76 (s, $1H_1$) ppm.

(H_2trz)[$OsCl_5$(Htrz)] (11). To triazole (15 mg, 0.22 mmol) in water (1.5 mL) was added 12 M hydrochloric acid (0.02 mL, 0.24 mmol). The resulting solution of triazolium chloride was then added to a solution of **8** (48 mg, 0.10 mmol) in water (4.8 mL). The reaction mixture produced red needle-like crystals. Yield: 28 mg, 56%. Anal. Calcd for $C_4H_7Cl_5N_6Os$ (M_r = 506.63 g/mol): C, 9.48; H, 1.39; N, 16.59. Found: C, 9.49; H, 1.23; N, 16.35. ESI-MS in MeOH (negative): m/z 436 $[Os^{IV}Cl_5(Htrz)]^-$, 401 $[Os^{III}Cl_4(Htrz)]^-$, 367 $[Os^{IV}Cl_5]^-$, 332 $[Os^{III}Cl_4]^-$. Solubility in water 4.4 mM at 298 K. IR, cm^{-1}: 621, 661, 743, 838, 877, 934, 970, 1027, 1058, 1150, 1258, 1300, 1413, 1518, 1560, 1602, 2807, 2848, 2916, 2955, 3124, 3521, 3601. UV−vis (H_2O), λ_{max}, nm (ε, M^{-1} cm^{-1}): 212 sh (117 773), 338 sh (4 890), 363 (8 229). ^1H NMR (d_6-DMSO, 500.32 MHz): δ −2.19 (s, 1H), 8.71 (s, $2H_{3,5}'$), 8.90 (brs) ppm.

{(Bu_4N)$_2$[$Os^{IV}Cl_6$]}$_2$·[$Os^{IV}Cl_4$(Him)$_2$] (12). To a solution of (H_2im)$_2$[$OsCl_6$] (100 mg, 0.18 mmol) in dry ethanol (10 mL) excess Bu_4NCl (153 mg, 0.55 mmol) was added. The suspension was stirred at 85 °C for 24 h. The volume of the solvent was then reduced to a quarter, and the reaction mixture was allowed to stand at −20 °C for 2 days. The orange crystals formed were filtered off, washed with diethyl ether (2 × 5 mL) and dried in vacuo. Yield: 80 mg, 58%. Anal. Calcd for $C_{70}H_{152}Cl_{16}N_8Os_3$ (M_r = 2243.80 g/mol): C, 37.47; H, 6.83; N, 4.99. Found: C, 37.49; H, 6.70; N, 4.93. ESI-MS in MeOH (negative): m/z 469 $[Os^{IV}Cl_4(Him)_2-H^+]^-$, 367 $[Os^{IV}Cl_5]^-$, 332 $[Os^{III}Cl_4]^-$. IR, cm^{-1}: 615, 653, 737, 880, 1025, 1065, 1100, 1135, 1259, 1323, 1378, 1474, 1547, 2873, 2958, 3164, 3251. UV−vis (C_2H_5OH), λ_{max}, nm (ε, M^{-1} cm^{-1}): 254 sh (19 949), 339 (49 763), 371 (45 578), 421 sh (7141). ^1H NMR (d_6-DMSO, 500.32 MHz): δ −0.52 (s, 1H), 0.95 (t, $24H_D$, J = 7.3 Hz), 1.32 (sxt, $16H_C$, J = 7.3 Hz), 1.58 (qui, $16H_B$, J = 7.5 Hz), 3.17 (t, $16H_A$, J = 8.3 Hz), 7.28 (s, 1H), 7.85 (s, 1H), 12.28 (s, $1H_1$) ppm. X-ray diffraction quality crystals were selected directly from the reaction vessel.

Physical Measurements. Elemental analyses were performed by the Microanalytical Service of the Institute of Physical Chemistry of the University of Vienna. IR spectra were obtained by using an ATR unit with a Perkin-Elmer 370 FTIR 2000 instrument (4000−400 cm^{-1}). UV−vis spectra were recorded on a Perkin-Elmer Lambda 20 UV−vis spectrophotometer using samples dissolved in water or ethanol. The aqueous solution behavior of **6**, **7**, and **9** with respect to hydrolysis was studied at 294 K over 24 h by UV−vis spectroscopy. Electrospray ionization mass spectrometry (ESI-MS) was carried out with a Bruker Esquire 3000 instrument (Bruker Daltonics, Bremen, Germany) by using methanol, methanol/acetonitrile, or water as solvents. Expected and measured isotope distributions were compared. Cyclic voltammogramms were measured in a three-electrode cell using a 2 mm diameter glassy carbon disk working electrode, a platinum auxiliary electrode and an $Ag|Ag^+$ reference electrode containing 0.1 M $AgNO_3$. Measurements were performed at room temperature using a EG&G PARC potentiostat/galvanostat model 273A. Deaeration of solutions was accomplished by passing a stream of argon through the solution for 5 min prior to the measurement and then maintaining a blanket atmosphere of argon over the solution during the measurement. The potentials were measured in 0.2 M (Bu_4N)[BF_4]/DMSO using [Fe(η^5-C_5H_5)$_2$] ($E_{1/2}^{ox}$ = +0.68 V vs NHE)[16] as internal standard and are quoted relative to NHE. Thermogravimetry was performed under nitrogen atmosphere on a Mettler Toledo TGA/SDTA851^e instrument. The ^1H, ^{13}C, and ^{15}N NMR spectra were recorded at 500.32, 125.81, and 50.68 MHz on a Bruker DPX500 (Ultrashield Magnet) in d_6-DMSO. 2D $^{13}C^1H$ HSQC, $^{15}N^1H$ HSQC, $^{13}C^1H$ HMBC, $^1H^1H$ COSY, and $^1H^1H$ NOESY experiments were performed for **1**, **2**, and **9**. Atom labeling with an apostrophe (Y_x') was introduced for assignments of azolium ion resonances in NMR spectra (Chart 1). Magnetic susceptibility data were collected on powdered samples with a SQUID-based sample magnetometer on a Quantum Design model MPMS instrument. All data were corrected for the diamagnetism of the ligands estimated from Pascal's constants.[17] Magnetic susceptibility measurements in solution were conducted on a Bruker DPX500 (Ultrashield Magnet) NMR spectrometer in d_6-DMSO by Evans method. The μ_{eff} calculated for 0.023 M Cu(acac)$_2$ (acac = acetylacetonate) solution in d_6-DMSO was 1.74 μ_B.

Crystallographic Structure Determination. X-ray diffraction measurements were performed on a Bruker X8 APEXII CCD diffractometer. Single crystals were positioned at 35, 40, 40, 40, 35, 35, and 35 mm from the detector, and 1983, 2366, 1789, 1414, 1449, 2620, and 1273 frames were measured, each for 50, 20, 40, 60, 40, 20, and 80 s over 1° scan width for **1**−**6** and **12**, correspondingly. The data were processed using SAINT software.[18] Crystal data, data collection parameters, and structure refinement details are given in Tables 1 and 2. The structures were solved by direct methods and refined by full-matrix least-squares techniques. Non-H atoms were refined with anisotropic displacement parameters. H atoms were inserted in calculated positions and refined with a riding model. The following software, personal computer and tables were used: structure solution, SHELXS-97;[19] refinement, SHELXL-97;[20] molecular diagrams, ORTEP;[21] Pentium IV; scattering factors.[22]

Cell Lines and Culture Conditions. CH1 (ovarian carcinoma, human) cells were donated by Lloyd R. Kelland (CRC Centre for Cancer Therapeutics, Institute of Cancer Research, Sutton, U.K.). A549 (non-small cell lung cancer, human) and SW480 (colon carcinoma, human) cells were kindly provided by Brigitte Marian (Institute of Cancer Research, Department of Medicine I, Medical

(16) Barrette, W. C., Jr.; Johnson, H. W., Jr.; Sawyer, D. T. *Anal. Chem.* **1984**, *56*, 1890–1898.
(17) Pascal, P. *Ann. Chim. Phys.* **1910**, *19*, 5–70.
(18) *SAINT-Plus, version 7.06a and APEX2*; Bruker-Nonius AXS Inc.: Madison, WI, 2004;
(19) Sheldrick, G. M., *SHELXS-97, Program for Crystal Structure Solution*; University of Göttingen: Göttingen, Germany, 1997.
(20) Sheldrick, G. M., *SHELXL-97, Program for Crystal Structure Refinement*; University of Göttingen: Göttingen, Germany, 1997.
(21) Johnson, G. K. *Report ORNL-5138*; Oak Ridge National Laboratory: Oak Ridge, TN, 1976.
(22) *International Tables for X-ray Crystallography*; Kluwer Academic Press: Dordrecht, The Netherlands, 1992; Vol. *C*, Tables 4.2.6.8 and 6.1.1.

Table 1. Crystal Data and Details of Data Collection for **1**−**5**

	1	**2**	**3**	**4**·CH_3OH	**5**·C_2H_5OH
empirical formula	$C_{19}H_{40}Cl_5N_3Os$	$C_{23}H_{42}Cl_5N_3Os$	$C_{19}H_{40}Cl_5N_3Os$	$C_{24}H_{46}Cl_5N_3OOs$	$C_{20}H_{45}Cl_5N_4OOs$
Fw	677.99	728.05	677.99	760.09	725.05
space group	$P\bar{1}$	$P\bar{1}$	$P2_1/n$	$P\bar{1}$	$P1$
a [Å]	10.6292(8)	9.8278(8)	10.7865(6)	10.2229(7)	9.6679(3)
b [Å]	11.4265(8)	10.9541(8)	19.3982(13)	11.2755(8)	10.4061(3)
c [Å]	11.7079(9)	14.7537(12)	13.3421(8)	14.9270(11)	15.1487(6)
α [deg]	68.717(4)	109.992(5)		74.902(4)	98.195(2)
β [deg]	85.748(4)	96.282(6)	109.892(3)	72.132(4)	103.674(2)
γ [deg]	83.527(3)	91.468(5)		78.163(4)	90.020(1)
V [Å^3]	1315.70(17)	1480.3(2)	2625.1(3)	1566.34(19)	1464.80(8)
Z	2	2	4	2	2
λ [Å]	0.71073	0.71073	0.71073	0.71073	0.71073
ρ_{calcd} [g cm^{-3}]	1.711	1.633	1.715	1.612	1.644
crystal size [mm^3]	0.25 × 0.10 × 0.10	0.10 × 0.10 × 0.06	0.10 × 0.07 × 0.03	0.14 × 0.08 × 0.02	0.30 × 0.30 × 0.02
T [K]	100	100	100	100	100
μ [mm^{-1}]	5.365	4.775	5.378	4.518	4.828
R_1[a]	0.0314	0.0282	0.0339	0.0377	0.0264
wR_2[b]	0.0742	0.0600	0.0806	0.0787	0.0669
GOF[c]	1.008	1.009	1.008	1.021	1.069

[a] $R_1 = \sum||F_o| - |F_c||/\sum|F_o|$. [b] $wR_2 = \{\sum w(F_o^2 - F_c^2)^2/\sum w(F_o^2)^2\}^{1/2}$. [c] GOF $= \{\sum[w(F_o^2 - F_c^2)^2]/(n-p)\}^{1/2}$, where n is the number of reflections and p is the total number of parameters refined.

Table 2. Crystal Data and Details of Data Collection for **6** and **12**

	6·$2H_2O$	**12**
empirical formula	$C_3H_8Cl_5N_2NaO_2Os$	$C_{70}H_{152}Cl_{16}N_8Os_3$
Fw	494.55	2243.80
space group	$P\bar{1}$	$P2_1/n$
a [Å]	6.5037(3)	11.1066(7)
b [Å]	6.8557(3)	16.2484(9)
c [Å]	13.5359(6)	26.7804(15)
α [deg]	96.816(3)	
β [deg]	91.235(2)	94.799(3)
γ [deg]	94.297(3)	
V [Å^3]	597.30(5)	4816.0(5)
Z	2	2
λ [Å]	0.71073	0.71073
ρ_{calcd} [g cm^{-3}]	2.750	1.547
crystal size [mm^3]	0.20 × 0.06 × 0.03	0.10 × 0.05 × 0.01
T [K]	100	100
μ [mm^{-1}]	11.803	4.431
R_1[a]	0.0203	0.0465
wR_2[b]	0.0547	0.0848
GOF[c]	1.099	0.974

[a] $R_1 = \sum||F_o| - |F_c||/\sum|F_o|$. [b] $wR_2 = \{\sum w(F_o^2 - F_c^2)^2/\sum w(F_o^2)^2\}^{1/2}$. [c] GOF $= \{\sum[w(F_o^2 - F_c^2)^2]/(n-p)\}^{1/2}$, where n is the number of reflections and p is the total number of parameters refined.

University of Vienna, Austria). Cells were grown in 75 cm^2 culture flasks (Iwaki/Asahi Technoglass) as adherent monolayer cultures in Minimal Essential Medium (MEM) supplemented with 10% heat-inactivated fetal bovine serum, 1 mM sodium pyruvate, and 2 mM L-glutamine (all purchased from Sigma-Aldrich) without antibiotics. Cultures were maintained at 37 °C in a humidified atmosphere containing 5% CO_2 and 95% air.

Cytotoxicity in Cancer Cell Lines. Cytotoxicity in the cell lines mentioned above was determined by the colorimetric MTT assay (MTT = 3-(4,5-dimethyl-2-thiazolyl)-2,5-diphenyl-2*H*-tetrazolium bromide, purchased from Fluka). Cells were harvested from culture flasks by trypsinization and seeded in 100 μL aliquots in MEM supplemented with 10% heat-inactivated fetal bovine serum, 1 mM sodium pyruvate, 2 mM L-glutamine, and 1% non-essential amino acids (100×) into 96-well microculture plates (Iwaki/Asahi Technoglass) in the following densities, to ensure exponential growth of untreated controls throughout the experiment: 1.5×10^3 (CH1), 4.0×10^3 (A549), and 2.5×10^3 (SW480) viable cells per well. Cells were allowed to settle and resume exponential growth in drug-free complete culture medium for 24 h, followed by the addition of dilutions of the test compounds in 100 μL/well of the same medium. After continuous exposure for 96 h, the medium was replaced by a 100 μL/well RPMI 1640 medium (supplemented with 10% heat-inactivated fetal bovine serum and 4 mM L-glutamine) plus 20 μL/well solution of MTT in phosphate-buffered saline (5 mg/mL) (all purchased from Sigma-Aldrich). After incubation for 4 h, medium/MTT mixtures were removed, and the formazan product formed by viable cells was dissolved in DMSO (150 μL/well). Optical densities at 550 nm were measured with a microplate reader (Tecan Spectra Classic), using a reference wavelength of 690 nm to correct unspecific absorption. The quantity of viable cells was expressed as percentage of untreated controls, and 50% inhibitory concentrations (IC_{50}) were calculated from concentration-effect curves by interpolation. Evaluation is based on at least two independent experiments, each comprising three replicates per concentration level.

Results and Discussion

Synthesis. Our previous investigation of the "$(H_2azole)_2[Os^{IV}Cl_6]$ − Hazole" system[3b,10,11] resulted in osmium(III)chlorido compounds of the general formulas $[Os^{III}Cl_2(Hazole)_4]Cl$ and $[Os^{III}Cl_3(Hazole)_3]$. The reduction occurred in boiling isoamyl alcohol or hexanol in the absence of any other reducing agent. In the case of the benzimidazole system we observed the formation of an intermediate species, namely, $[Os^{IV}Cl_4(Hbzim)_2]$. This result prompted us to explore the following scheme for the synthesis of azolepentachloridoosmate(IV) complexes:

$$(H_2azole)_2[Os^{IV}Cl_6] \xrightarrow{-HCl} (H_2azole)[Os^{IV}Cl_5(Hazole)] \xrightarrow{-HCl} [Os^{IV}Cl_4(Hazole)_2]$$

Such transformations are known as Anderson rearrangements[23] and can be performed both in the solid state and in solution. As starting materials the $(H_2azole)_2[Os^{IV}Cl_6]$

(23) Davies, J. A.; Hockensmith, C. M.; Kukushkin, V. Yu.; Kukushkin, Yu. N. *Synthetic Coordination Chemistry − Principles and Practice*; World Scientific Pub. Co.: New Jersey, 1995; pp 392−396.

(Hazole = Him, Hpz, Hind, Hbzim) compounds were used.[3b] By following the reported protocol[3b] the triazole analogue $(H_2trz)_2[Os^{IV}Cl_6]$ was synthesized in 94% yield (see Supporting Information).

The performed thermogravimetric analyses for $(H_2azole)_2[Os^{IV}Cl_6]$ did not confirm the expected stepwise liberation of one and then another molecule of HCl, which would have allowed the isolation of the reaction product after elimination of the first molecule of HCl. However, this approach proved to be more appropriate for the production of $[Os^{IV}Cl_4(Hazole)_2]$. These latter compounds are of non-electrolytic type, insoluble in aqueous and other biocompatible media. Since we are primarily interested in water-soluble versions of compounds for the investigation of their biological properties, our research was focused on the synthesis of $[Os^{IV}Cl_5(Hazole)]^-$ species.

To quench the Anderson rearrangement after the first step, we performed the reaction in the presence of tetrabutylammonium chloride, thereby inducing the precipitation of $[Os^{IV}Cl_5(Hazole)]^-$ complexes as tetrabutylammonium salts. The reactions were carried out in boiling ethanol. As a result the complexes **1**, **2**, **4**, and **5** were synthesized in 24−79% yields. The synthesis of **4** was accompanied by concurrent formation of *trans*-$[Os^{IV}Cl_4(Hbzim)_2]$. The reaction with $(H_2im)_2[Os^{IV}Cl_6]$ ended up by precipitation of $\{(Bu_4N)_2[Os^{IV}Cl_6]\}_2$-$[Os^{IV}Cl_4(Him)_2]$ (**12**) in 58% yield. The reaction of the imidazole system carried out in isoamyl alcohol at 100 °C afforded *trans*-$[Os^{IV}Cl_4(Him)_2]$ and a minor amount of **3**. These results indicate that the $[Os^{IV}Cl_5(Him)]^-$ species is formed as an intermediate, which is immediately converted into *trans*-$[Os^{IV}Cl_4(Him)_2]$. The transformations in isoamyl alcohol are slower, allowing the isolation of the $[Os^{IV}Cl_5(Him)]^-$ species.

The observed reactivity of $(H_2azole)_2[Os^{IV}Cl_6]$ complexes in boiling ethanol agrees well with the electron donating properties of the azole ligands (Him > Hbzim > Htrz > Hpz > Hind),[24] which account for the deeper substitution for imidazole and benzimidazole systems resulting in the formation of single and double substituted products. In the case of indazole and benzimidazole the corresponding complexes $(Bu_4N)[Os^{IV}Cl_5(Hazole)]$ were isolated in higher yields because of poorer solubility of these compounds.

To improve the aqueous solubility of $(Bu_4N)[Os^{IV}Cl_5(Hazole)]$ compounds (Hazole = Hpz, Htrz, Hind) and to avoid the toxicity caused by the tetrabutylammonium cation, they were converted into their sodium (**6**−**8**) and azolium salts (**9**−**11**). The sodium salts were obtained in 91−98% yields by stirring the aqueous or aqueous/ethanolic solutions of **1**, **2**, and **5** with DOWEX Marathon C ion exchanger resin (1 g for 10 mg of the corresponding complex) for 30 min. These were further reacted with the in situ prepared azolium chloride in 1:1 or 1:2 molar ratio in water to give $(H_2azole)[Os^{IV}Cl_5(Hazole)]$ (**9**−**11**) in 52−78% yields.

Crystal Structures. The crystal structures of **1**−**5** contain essentially octahedral complexes of the general formula $[Os^{IV}Cl_5(Hazole)]^-$ (Figures 1−3). Table 3 quotes some geometrical details of the complexes studied. Complexes **1**, **2**, and **4** crystallized in the triclinic space group $P\bar{1}$, while **3** and **5** in the monoclinic space group $P2_1/n$ and triclinic noncentrosymmetric space group $P1$, respectively. The asymmetric unit of **5**, in contrast to those of **1**−**4**, consists of two crystallographically independent complex anions, (see Figure 3c, Table 3) with well-comparable metric parameters.

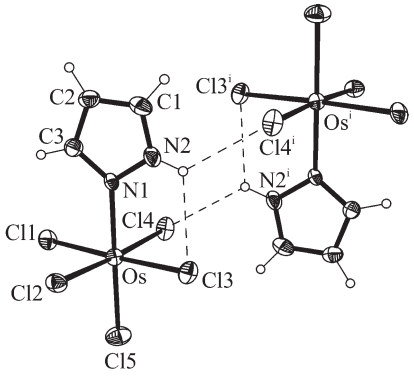

Figure 1. ORTEP view of the $[Os^{IV}Cl_5(Hpz)]^-$ anion involved in hydrogen bonding interactions with the adjacent complex anion in **1**, showing the atom-numbering schemes. Thermal ellipsoids are drawn at 50% probability level. Atoms marked i are at the symmetry positions $(-x+2, -y+2, -z+1)$. Hydrogen bonding parameters: N2−H···Cl3 and N2−H···Cl4^i (N2−H 0.88, H···Cl3 2.580, N2···Cl3 3.093 Å, N2HCl3 118.04°, H···Cl4^i 2.693, N2···Cl4^i 3.296 Å, N2HCl4^i 126.71°).

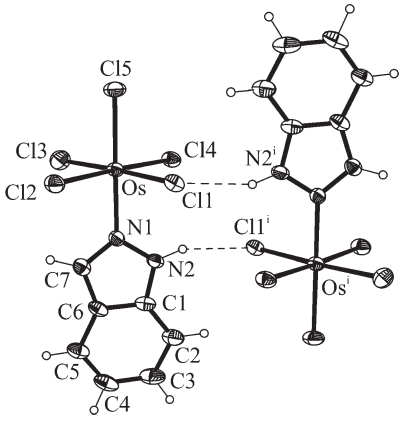

Figure 2. ORTEP view of the $[Os^{IV}Cl_5(Hind)]^-$ anion involved in hydrogen bonding interactions with the adjacent complex anion in **2**, showing the atom-numbering schemes. Thermal ellipsoids are drawn at 50% probability level. Atoms marked i are at the symmetry positions $(-x+1, -y+1, -z+1)$. Hydrogen bonding parameters: N2−H···Cl1^i (N2−H 0.88, H···Cl1^i 2.611, N2···Cl1^i 3.354 Å, N2HCl1^i 142.81°).

Intra- and intermolecular hydrogen bonding interactions are evident in the crystal structure of **1** (Figure 1).

The azole ligand coordinated to osmium(IV) via N1 is tilted relative to the mean plane through OsN1Cl3Cl5Cl1,

The Os−Cl bonds in **1**−**5** are commonly significantly longer than in $(Ph_4P)[Os^{V}Cl_6]$[25] at 2.252(4)−2.295(2) or $(Et_4N)[Os^{V}Cl_6]$[26] at 2.295(3)−2.308(2) Å and well-comparable to those in $(HPPh_3)_2[Os^{IV}Cl_6]\cdot DMF$[27] at 2.330(5)−2.340(5) Å.

(24) Reisner, E.; Arion, V. B.; Keppler, B. K.; Pombeiro, A. J. L. *Inorg. Chim. Acta* **2008**, *361*, 1569–1583.

(25) Kim, E. E.; Eriks, K.; Magnuson, R. *Inorg. Chem.* **1984**, *23*, 393–397.

(26) Krebs, B.; Henkel, G.; Dartmann, M.; Preetz, W.; Bruns, M. *Z. Naturforsch.* **1984**, *39b*, 843–849.

(27) Robinson, P. D.; Hinckley, C. C.; Matusz, M.; Kibala, P. A. *Acta Crystallogr.* **1988**, *C44*, 619–621.

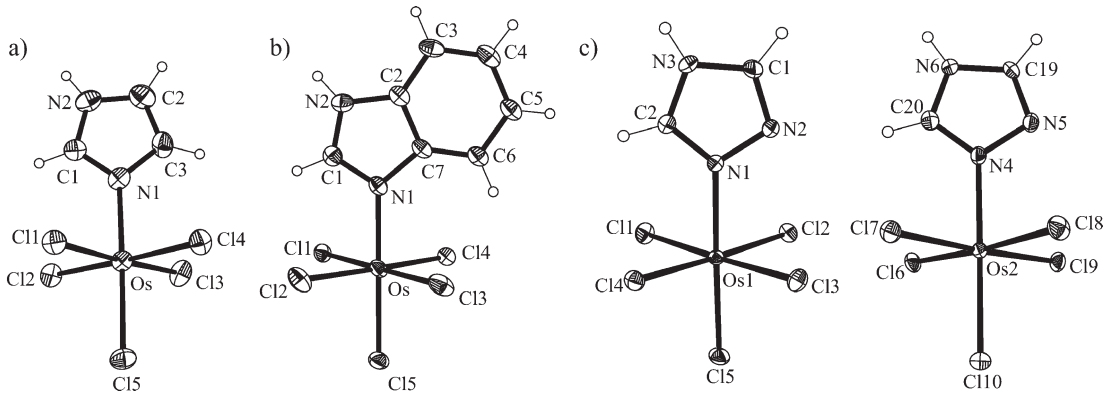

Figure 3. ORTEP view of the $[Os^{IV}Cl_5(Him)]^-$ anion (a) in **3**, the $[Os^{IV}Cl_5(Hbzim)]^-$ anion (b) in $\mathbf{4}\cdot CH_3OH$, and of the two crystallographically independent $[Os^{IV}Cl_5(Htrz)]^-$ anions (c) in $\mathbf{5}\cdot C_2H_5OH$, showing the atom-numbering schemes. Thermal ellipsoids are drawn at 50% probability level.

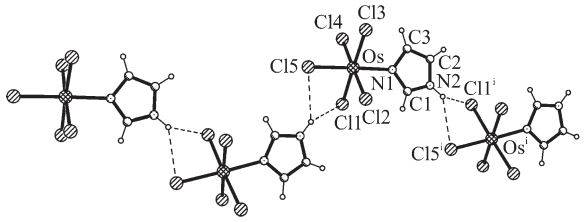

Figure 4. Part of the crystal structure of **3**, showing the 1D arrangement of osmium(IV) complexes via intermolecular hydrogen-bonding interactions. Atoms marked i are at the symmetry positions ($x - 0.5$, $-y + 0.5$, $z - 0.5$). Hydrogen-bonding parameters: N2−H···Cl1^i and N2−H···Cl5^i (N2−H 0.88, H···Cl1^i 2.652, N2···Cl1^i 3.340 Å, N2HCl1^i 135.78; H···Cl5^i 2.679, N2···Cl5^i 3.380 Å, N2HCl5^i 137.44°).

OsN1Cl2Cl4Cl5, OsN1Cl2Cl5Cl4 and Os1N1Cl3Cl5Cl1, the corresponding dihedral angles being at 19.3(2), 38.89(6), 39.6(2), and 41.23(9)° in **1**−**4**, respectively (Figures 1−3). The triazole ligands in two crystallographically independent complex anions in **5**, which are bonded to osmium atoms via N1 and N4, are tilted relative to the mean planes through Os1N1Cl1Cl3Cl5 and Os2N4Cl7Cl9Cl10 at 45.5(2) and 38.5(1)°, respectively (Figure 3).

Intermolecular hydrogen bonding interactions in **2** are shown in Figure 2.

The complex anions $[Os^{IV}Cl_5(Him)]^-$ in **3** form a 1D chain via intermolecular hydrogen bonding interactions of the type N−H···Cl (Figure 4).

The molecule of CH_3OH in the crystal structure of $\mathbf{4}\cdot CH_3OH$, acts as proton donor in a bifurcated hydrogen bond to chloride ligands Cl2^i and Cl5^i and as proton acceptor in the hydrogen bond N2−H···O1 (Figure 5).

An interesting feature is the stabilization of the 4*H* tautomeric form of the 1,2,4-triazole in $\mathbf{5}\cdot C_2H_5OH$ through bonding of the ligand via N2 in the nomenclature used for 1*H*- or 4*H*-1,2,4-triazole. Note that in the solid Htrz crystallizes exclusively as a 1*H*-tautomer.[28,29] This rare behavior was also documented recently for (H_2trz)-[*cis*-$Ru^{III}Cl_4(Htrz)_2]\cdot H_2O$,[30] (Ph_3PCH_2Ph)[*trans*-$Ru^{III}Cl_4(Htrz)_2$][30], and *mer*-$[Ru^{III}Cl_3(Htrz)_3]$.[31] The established mode of coordination of 1,2,4-triazole is also corroborated by participation of all non-coordinated nitrogen atoms in strong hydrogen bonding interactions, as shown in Figure 6. The atoms N3 and N6 act as proton donors to N5 and N2, Cl2, correspondingly.

Complex **6** crystallized in the triclinic centrosymmetric space group $P\bar{1}$. The crystal structure (Figure 7) shows that it is an infinite 1D chain consisting of centrosymmetric dimers of heterometallic (Os−Na) entities running along *a* axis. The octahedral osmium(IV) atom is bound to five chlorido ligands and a pyrazole molecule through nitrogen atom N1. The Cl1 and Cl5 atoms act as bridging ligands between osmium(IV) and the neighboring sodium cation, which is six-coordinate. The latter is also bound with two water molecules via O1 and O2, which act as bridging ligands to two other centrosymmetry related sodium cations. The inversion center resides in the middle of the vector connecting the two atoms Na and Na^i ($x+1$, $y+1$, $z+1$). The Na−O1 and Na−O2 distances of 2.346(4) and 2.340(4) Å, respectively, are well comparable with those found in penta-μ-aqua-disodium(I) bis(dimethylarsenate), $\{[Na_2(H_2O)_5](C_2H_6AsO_2)_2\}_n$ at 2.317(3)−2.422(2) Å.[32]

Complex **12** crystallized in the monoclinic space group $P2_1/n$. The crystal structure of **12** consists of neutral complexes *trans*-$[Os^{IV}Cl_4(Him)_2]$ and ionic complexes $(Bu_4N)_2[Os^{IV}Cl_6]$ in 1:2 molar ratio. The neutral complex is octahedral (Figure 8). The osmium(IV) atom is bound to four chlorido ligands in the equatorial plane and to two monodentate imidazole ligands in axial positions. The Os−N1 bond of 2.058(6) Å is significantly shorter than the Ru−N3 bond of 2.081(5) Å in $[P(C_6H_5)_4][Ru^{III}Cl_4(5\text{-}NO_2Him)_2]$[33] as well as the Ru−N1 and Ru−N3 bonds of 2.0687(12) and 2.0682(12) Å, respectively, in *trans*-$[Ru^{III}Cl_2(Him)_4]Cl$.[31] The Os−Cl1 bond of 2.3354(19) Å is significantly longer than the Os−Cl2 bond of 2.310(2) Å because of partake of Cl1 as a proton acceptor in two intramolecular hydrogen bonding interactions of the type Cl1···H−C1 and Cl1···H−C3^i($-x+2$, $-y+1$, $-z+2$). At the same time C1 acts as a proton donor in intermolecular hydrogen bonding of the complex *trans*-$[Os^{IV}Cl_4(Him)_2]$ with $[Os^{IV}Cl_6]^{2-}$ (Figure 8), where

(28) Jeffrey, G. A.; Ruble, J. R.; Yates, J. H. *Acta Crystallogr.* **1983**, *B39*, 388–394.
(29) Fuhrmann, P.; Koritsanszky, T.; Luger, P. *Z. Kristallogr.* **1997**, *212*, 213–220.
(30) Arion, V. B.; Reisner, E.; Fremuth, M.; Jakupec, M. A.; Keppler, B. K.; Kukushkin, V. Yu.; Pombeiro, A. J. L. *Inorg. Chem.* **2003**, *42*, 6024–6031.
(31) Reisner, E.; Arion, V. B.; Eichinger, A.; Kandler, N.; Giester, G.; Pombeiro, A. J. L.; Keppler, B. K. *Inorg. Chem.* **2005**, *44*, 6704–6716.
(32) Lennartson, A.; Håkansson, M. *Acta Crystallogr.* **2008**, *C64*, m13–m16.
(33) Anderson, C.; Beauchamp, H. L. *Inorg. Chim. Acta* **1995**, *233*, 33–41.

Table 3. Selected Bond Distances (Å) in **1**−**5**

	1	**2**	**3**	**4**·CH_3OH	**5**·C_2H_5OH
Os−N1 [Os1−N1, Os2−N4]	2.094(3)	2.068(3)	2.084(4)	2.076(4)	[2.086(4), 2.081(4)]
Os−Cl_{axial} [Os1−Cl5, Os2−Cl10]	2.3132(9)	2.3332(10)	2.3445(13)	2.3549(12)	[2.3270(11), 2.3136(12)]
Os−$Cl_{equatorial}$(av) [Os1−Cl1−4, Os2−Cl6−9]	2.333(11)	2.325(11)	2.331(21)	2.332(4)	[2.326(10), 2.328(11)]

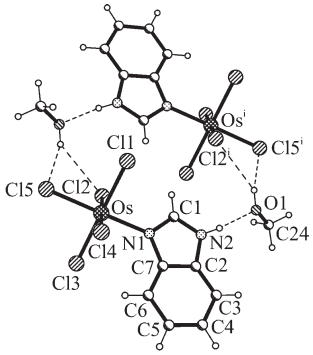

Figure 5. Part of the crystal structure of **4**·CH_3OH,, showing the intermolecular hydrogen-bonding interactions between complex anions and solvent molecules. Atoms marked i are at the symmetry positions ($-x+1$, $-y+2$, $-z+1$). Hydrogen-bonding parameters: N2−H···O1 (N2−H 0.88, H···O1 1.886, N2···O1 2.763 Å, N2HO1 174.08°) and O1−H···$Cl2^{i}$ and O1−H···$Cl5^{i}$ (O1−H 0.84, H···$Cl2^{i}$ 2.829, O1···$Cl2^{i}$ 3.473 Å, O1H$Cl2^{i}$ 134.90; H···$Cl5^{i}$ 2.507, O1···$Cl5^{i}$ 3.235 Å, O1H$Cl5^{i}$ 145.44°).

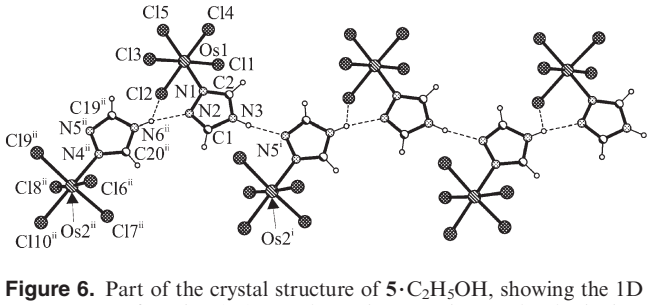

Figure 6. Part of the crystal structure of **5**·C_2H_5OH, showing the 1D arrangement of osmium(IV) complexes via strong intermolecular hydrogen-bonding interactions. Atoms marked i and ii are at the symmetry positions (x, $y+1$, z) and ($x+1$, $y-1$, z), respectively. Hydrogen-bonding parameters: N3−H···$N5^{i}$ (N3−H 0.88, H···$N5^{i}$ 1.920, N3···$N5^{i}$ 2.792 Å, N3HN5 170.39°), $N6^{ii}$−H···N2, and $N6^{ii}$−H···Cl2 ($N6^{ii}$−H 0.88, H···N2 1.918, $N6^{ii}$···N2 2.785 Å, $N6^{ii}$HN2 168.0°; H···Cl2 2.926, $N6^{ii}$···Cl2 3.344 Å, $N6^{ii}$HCl2 111.03°).

$Cl6^{ii}$ acts as a proton acceptor. In addition, N2 acts as a proton donor and $Cl3^{ii}$ and $Cl8^{ii}$ as proton acceptors in an intermolecular bifurcated hydrogen bond between the two species (Figure 8). The elongation of the bonds Os2−Cl3 and Os2−Cl6 of 2.3685(18) and 2.3487(19), correspondingly, as compared to Os2−Cl4, Os2−Cl5, and Os2−Cl7 of 2.3299(19), 2.3291(18), and 2.3350(19) Å, respectively, is obvious.

NMR Spectra. The ^{1}H and ^{13}C NMR spectra of the reported compounds show signals due to $(Bu_4N)^+$ (**1**, **2**, **4**, **5**, **12**) or $(H_2azole)^+$ (**9**−**11**) cations and coordinated azole heterocycles (**1**−**12**, but not **3**).

The ^{1}H NMR spectrum of $(Bu_4N)^+$ (**1**, **2**, **4**, **5**, **12**) is well resolved and displays, as expected, a triplet for the CH_3 group (D) at 0.95 ppm, a sextet for the CH_2 group (C) at 1.32 ppm, a quintet for the CH_2 group (B) at 1.58 ppm, and a triplet for the CH_2 group (A) at 3.17 ppm with integration ratio 3:2:2:2 (for atom labeling see Chart 1). The ^{13}C{^{1}H} NMR spectra of the $(Bu_4N)^+$ cation (**1**, **2**) show four signals: one for CH_3 at 14.1 (C_D) ppm and three for CH_2 at 19.8 (C_C), 23.7 (C_B), and 58.4 (C_A) ppm.

^{1}H NMR spectra of azolium cations reveal a set of split signals which is typical for a protonated azole heterocycle: two singlets for the pyrazolium cation in **9** at 6.31 and 7.68 ppm with relative intensities 1:2 ($1H_4'$, $2H_{3,5}'$), in accord with C_2 molecular symmetry for this cation; two triplets at 7.11 ($1H_5'$) and 7.34 ($1H_6'$) ppm, two doublets at 7.53 ($1H_7'$) and 7.75 ppm ($1H_4'$), and one singlet at 8.08 ppm ($1H_3'$) for the indazolium cation in **10**; one singlet at 8.71 ppm ($H_{3,5}'$) for the triazolium cation in **11**, in line with its C_2 own symmetry.

The assignment of the protons and carbon atoms in coordinated azoles is hindered because of their coordination to paramagnetic (low-spin d^4) osmium(IV). The paramagnetism causes broadening of the signals and shift to negative values, especially for the protons which are closer to the metal center. It should, however, be noted that the effect of the paramagnetic center is not the same for complexes with different azole heterocycles. Some of them have ^{1}H NMR spectra with resonances as sharp as those observed in diamagnetic compounds and shifted very little as compared with diamagnetic complexes. We succeeded to obtain two-dimensional NMR spectra for the pyrazole compounds **1** (^{15}N,^{1}H HSQC, ^{13}C,^{1}H HSQC) and **9** (^{15}N,^{1}H HSQC, ^{13}C,^{1}H HSQC, ^{13}C,^{1}H HMBC) and for the indazole species **2** (^{15}N,^{1}H HSQC, ^{13}C,^{1}H HSQC, ^{13}C,^{1}H HMBC, ^{1}H,^{1}H NOESY, ^{1}H,^{1}H COSY) (see Supporting Information, Figures S5−S15).

Pyrazole Compounds. The H_1 proton of the ligand was identified at 15.71 ppm from the ^{15}N,^{1}H HSQC plot (**1**, **9**). Because of the C_s own symmetry of the coordinated pyrazole, the H_3 and H_5 signals in the ^{1}H NMR spectra of **1**, **6**, and **9** do not overlap, as it is the case for the pyrazolium cation. The resonance signals H_3, H_4, and H_5 are observed as singlets at −2.75, −2.48, and 6.34 ppm for **6** and at −2.71, −2.44, and 6.39 ppm for **1** and **9**. In the ^{13}C{^{1}H} NMR spectra of **1** and **9** the carbon resonances for C_3, C_4, and C_5 are displayed at 71.08 {6.39}, 180.92 {−2.71}, 191.31 {−2.44} and 71.18 {6.39}, 181.33 {−2.71}, 191.99 {−2.44} ppm, respectively. In addition, the pyrazolium cation in **9** gives two C*H* signals at 106.16 (C_4') and 134.25 ($C_{3,5}'$) ppm. The ^{13}C,^{1}H HMBC plot of **9** does not clarify the assignment of C_3, C_4, C_5 and H_3, H_4, H_5 because of the same number of cross-signals for these carbon atoms and protons (two cross-peaks for every atom). H_1 has C*H* couplings with C_3, C_4, and C_5.

Indazole Compounds. The ^{1}H NMR signals of the coordinated indazole in **2**, **7**, and **10** have the same chemical shifts. Therefore, 2D NMR experiments were performed for **2**, and the assignments made were also applied to **7** and **10**. The multiplicity of ligand ^{1}H signals in the ^{1}H NMR spectrum is the same as for the metal-free indazole. From the ^{15}N,^{1}H HSQC plot H_1 is seen at 17.76 ppm. Another singlet, H_3, is observed at −4.54 ppm. The ^{1}H,^{1}H NOESY plot shows a cross-peak of H_7 with H_1,

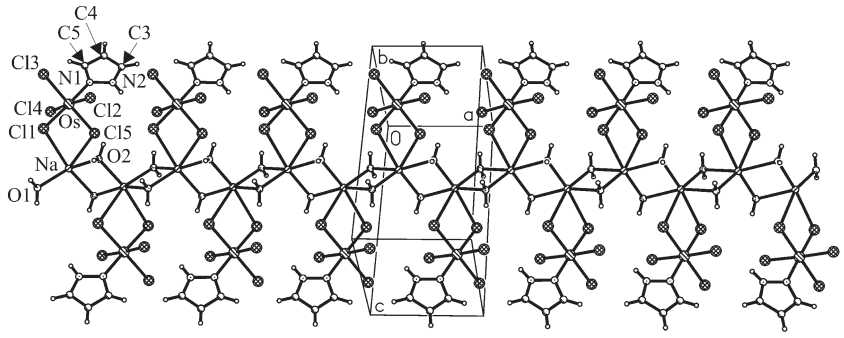

Figure 7. Projection of a part of the crystal structure of $[Na(H_2O)_2OsCl_5(Hpz)]_n$ on the *ac* plane of the unit cell, showing the formation of an infinite 1D chain in $\mathbf{6}\cdot 2H_2O$.

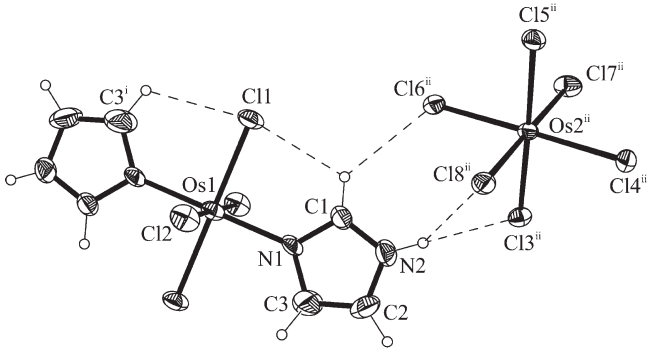

Figure 8. ORTEP view of the fragment of the crystal structure of **12**, showing intra- and intermolecular hydrogen bonding interactions between the complex *trans*-$[Os^{IV}Cl_4(Him)_2]$ and the complex anion $[Os^{IV}Cl_6]^{2-}$ with atom-numbering scheme. The thermal displacement ellipsoids are drawn at 50% probability level. Hydrogen bonding parameters: Cl1···H−C1 [Cl1···H 2.565, Cl1···C1 3.117, H−C1 0.95 Å, Cl1HC1 117.2°], Cl1···H−C3^{i} [Cl1···H 2.737, Cl1···C3^{i} 3.216, H−C3^{i} 0.95 Å, Cl1HC3^{i} 112.1°], C1−H···Cl6^{ii} [C1−H 0.95, H···Cl6^{ii} 2.671, C1···Cl6^{ii} 3.395 Å, C1HCl6^{ii} 133.4°], N2−H···Cl3^{ii} and N2−H···Cl8^{ii} [N2−H 0.88, H···Cl3^{ii} 2.471, N2···Cl3^{ii} 3.314 Å, N2HCl3^{ii} 160.64°; H···Cl8^{ii} 2.925, N2···Cl8^{ii} 3.491 Å, N2HCl8^{ii} 123.77°]. Atoms marked i are at the symmetry positions $x+2, y+1, z+2$, and those marked ii at the symmetry positions $x+1, y+1, z+1$.

and another resulting from coupling of H_4 with H_3. The cross-peaks in the $^1H,^1H$ COSY plot indicate H_4-H_5 and H_6-H_7 couplings. Therefore two doublets are due to H_7 (10.84 ppm) and H_4 (5.89 ppm) protons, while two triplets are due to H_6 (3.08 ppm) and H_5 (8.24 ppm). In the $^{13}C\{^1H\}$ NMR spectrum four C*H* signals for C_7, C_5, C_4, C_6 are seen at 81.88, 106.16, 139.58, and 163.74 ppm, correspondingly. The unresolved C_3 signal is detected at 200.66 ppm from the $^{13}C,^1H$ HSQC plot. In addition, two carbon signals originate from the quaternary carbons C_9 and C_8. In the $^{13}C,^1H$ HMBC plot one of them at 75.94 ppm shows five cross-peaks with all protons but H_6, whereas the second at 173.67 ppm reveals four cross-peaks, but no cross-peaks with H_5 and H_7. Taking into account that the couplings through four bonds, such as C_9-H_6 and C_8-H_5, are most likely undetectable, we can suppose that C_9 displays a signal at 75.94 ppm, while C_8 at 173.67 ppm.

Magnetic Properties. Complex **5** is paramagnetic at 300 K in the solid state (μ_{eff} = 1.86 μ_B). The magnetic moment is temperature-dependent, decreasing continuously with temperature and reaching the value of 0.40 μ_B at 2 K (see Supporting Information, Figure S19). This behavior indicates a non-magnetic ground state resulting from antiparallel coupling of the effective orbital moment $L = 1$ of the t_2 shell with the total spin $S = 1$ of the ground t_2^4 configuration, induced by spin−orbit coupling on Os(IV) in octahedral geometry. Given a very large spin−orbit coupling constant on the osmium ion (> 5000 cm^{-1}), the reduction of symmetry caused by axial ligands will not affect the character of the ground state, which thus will remain non-degenerate (non-magnetic) in the real geometry too (Figure 6). Measurement of the same complex in DMSO by Evans method[34,35] resulted in an increase of the effective magnetic moment (3.18 μ_B at 297 K). Similar behavior has been also documented in the literature[36] for magnetically diluted hexahalogenidoosmates(IV). Detailed magnetic studies are underway in our laboratory and will be reported in due course.

Electrochemical Behavior. The cyclic voltammograms (CVs) of the complexes **1**, **2**, **4**, and **5** in DMSO (0.2 M (n-Bu_4N)[BF_4]/DMSO) at a carbon disk working electrode, recorded with a scan rate of 0.2 V/s, display a reversible one-electron reduction wave attributed to the $Os^{IV} \rightarrow Os^{III}$ process with potential values ranging from −0.03 to 0.12 V and an irreversible single electron reduction wave (I^{red}) attributed to the $Os^{III} \rightarrow Os^{II}$ process with E_p potential values between −1.78 and −1.39 V versus NHE (Figure 9, Table 4 and Supporting Information, Figures S16 and S18). The redox waves Os^{IV}/Os^{III} are characterized by a peak-to-peak separation (ΔE_p) of 69−87 mV and an anodic peak current (i_{pa}) that is almost equal to the cathodic peak current (i_{pc}), as expected for reversible electron transfer processes. The one-electron nature of the electron transfer processes was verified by comparing the peak current height (i_p) with that of standard ferrocene/ferrocenium couples under identical experimental conditions. The reduction potentials Os^{IV}/Os^{III} are in the following order: $E_{1/2}(\mathbf{2}) > E_{1/2}(\mathbf{5}) > E_{1/2}(\mathbf{1}) > E_{1/2}(\mathbf{4})$, which agrees quite well with the relative electron-donating character of the azole ligands [E_L(Hind) > E_L(Hpz) > E_L(Htrz) > E_L(Hbzim)][24] and their basicity [pK_a(H_2ind$^+$) < pK_a(H_2trz$^+$) < pK_a(H_2pz$^+$) < pK_a(H_2-bzim$^+$)][3b,37−39] (Table 4). The reduction potential for

(34) Evans, D. F. *J. Chem. Soc.* **1959**, 2003–2005.
(35) Sur, S. K. *J. Magn. Reson.* **1989**, *82*, 169–173.
(36) Greenslade, D. J. *J. Chem. Soc. A* **1968**, *4*, 834–836.
(37) Potts, K. T. *Chem. Rev.* **1961**, *61*, 87–127.
(38) Catalán, J.; Claramunt, R. M.; Elguero, J.; Laynez, J.; Menéndez, M.; Anvia, F.; Quian, J. H.; Taagepra, M.; Taft, R. W. *J. Am. Soc. Chem* **1988**, *110*, 4105–4111.
(39) Reedijk, J. Heterocyclic Nitrogen-Donor Ligands. In *Comprehensive Coordination Chemistry*; Wilkinson, G., Gillard, R. D., McCleverty, J. A., Eds.; Pergamon Press: Elmsford; NY, 1987; Vol. *2*, pp 73−98.

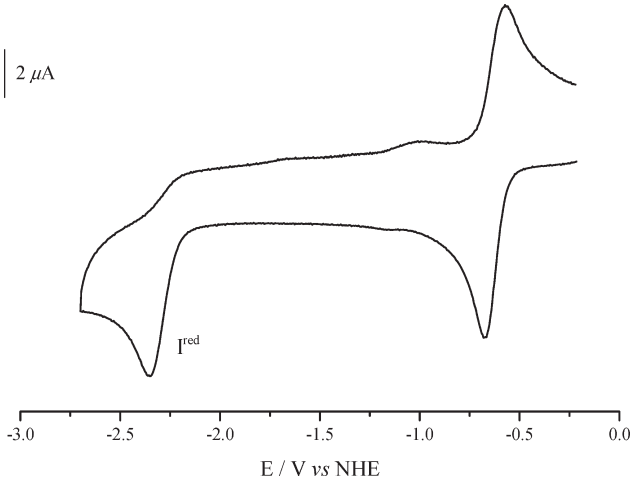

Figure 9. Cyclic voltammogram of 0.2 M **1** in DMSO at a carbon disk working electrode and a scan rate of 0.2 V/s, starting the scan in cathodic direction.

$Os^{III} \rightarrow Os^{II}$ was calculated using Lever's equation[40] (eq 1) [E_L(Cl) = −0.24,[41] E_L(Hpz) = 0.20,[41] E_L(Hbzim) = 0.1,[41] E_L(Hind) = 0.26,[42] E_L(Htrz) = 0.18,[43] $S_M(Os^{III}/Os^{II})$ = 1.01,[41] $I_M(Os^{III}/Os^{II})$ = −0.40[41]].

$$E = S_M \sum E_L + I_M \quad (1)$$

The values of E_{calc} for Os^{III}/Os^{II} using this formula agree quite well with the E_p values measured for Os^{III}/Os^{II} (Table 4).

Aqueous Solubility and Resistance to Hydrolysis. The aqueous solubility of the complexes **6**−**11** at 298 K varies from 1.3 mM (**10**) to 34.3 mM (**6**), depending on the coordinated azole heterocycle and cation identity. The sodium salts showed higher aqueous solubility than the analogous azolium salts. The aqueous solution behavior of **6**, **7**, and **9** with respect to hydrolysis was studied at 294 K over 24 h by UV−vis spectroscopy. The complexes remain intact in aqueous solution, as can be seen from their electronic absorption spectra (Figure 10 and Supporting Information, Figures S1 and S2).

Immediate hydrolysis was excluded, since the parent peak at m/z 434 for $[Os^{IV}Cl_5(Hpz)]^-$ was observed in the negative ion ESI mass spectrum of the aqueous solution of **9** after 24 h.

Cytotoxicity in Cancer Cell Lines. Cytotoxicity of compounds **6**−**11** was assessed by means of a colorimetric microculture assay (MTT assay) in three human cancer cell lines. The generally more chemosensitive CH1 (ovarian carcinoma) cells are somewhat, but not more than 3.4 times, more sensitive to these compounds than the least sensitive A549 (non-small cell lung cancer) cells, based on comparison of IC_{50} levels (Table 5).

The following structure−activity relationships can be inferred from the concentration-effect curves depicted in Figure 11: Variation of the azole ligand has marked

Table 4. Cyclic Voltammetric Data for **1**, **2**, **4**, and **5**

complex	E_p Os(III/II)	$E_{1/2}$ Os(IV/III)[a], (ΔE_p)[b]	E_{calc}	pK_a (H_2azole$^+$)
1	−1.66	0.03 (75)	−1.41	2.64
2	−1.39	0.12 (69)	−1.35	1.25
4	−1.78	−0.03 (72)	−1.51	5.63
5	−1.50	0.05 (87)	−1.43	2.55

[a] Potentials $E_{1/2}$ ($E_{1/2}$ = (E_{pa} + E_{pc})/2, where E_{pa} and E_{pc} are the anodic and cathodic peak potentials, are given in V and measured at a scan rate of 0.2 V/s in DMSO, using ferrocene as internal standard, and are quoted relative to NHE. [b] ΔE_p values (ΔE_p = E_{pa} − E_{pc}) are given in mV.

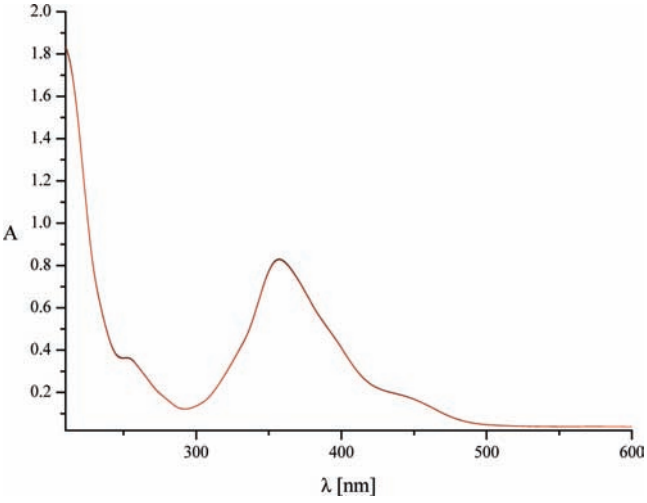

Figure 10. UV−vis spectra of an aqueous solution of **9**, measured immediately after dissolution of the sample and 24 h thereafter.

consequences for biological activity within the series of complexes with a sodium counterion. Cytotoxic potency decreases in the following rank order, depending on the azole ligand: pyrazole (**6**) > indazole (**7**) > triazole (**8**), whereas the differences are much less pronounced within the series of azolium analogues (**9**, **10**, **11**), which generally have modest cytotoxic potencies, with IC_{50} values varying only in a small range of 10^{-4} M concentrations in all three cell lines. This implies that exchange of the counterion influences biological activity to a different extent. In the case of the pyrazole complexes (**6** vs **9**), formal replacement of the azolium cation with sodium results in a 3.0- to 5.8-fold enhancement of cytotoxicity to IC_{50} values in the 10^{-5} M range, while the difference is reduced to factors of 1.3−2.0 in the indazole complexes (**7** vs **10**) and completely abolished in the triazole complexes (**8** vs **11**). These findings are remarkable because they contrast with observations made with $[Ru^{III}Cl_4(Hind)_2]^-$, which is less cytotoxic in the form of the sodium salt.[44] An explanation is not obvious because the counterion is unlikely to be involved in the molecular effects accounting for cytotoxicity. Experiments are ongoing to clarify whether a different extent of cellular uptake may contribute to these differences.

Comparison with the ruthenium(III) compound $(H_2ind)_2[RuCl_5(Hind)]$ (IC_{50} = 35 μM and 37 μM in CH1 and SW480 cells, respectively)[9] reveals that the

(40) Lever, A. B. P.: Dodsworth, E. S. *Inorganic Electronic Structure and Spectroscopy*; Wiley: New York, 1999; pp 277−290.
(41) Lever, A. B. P. *Inorg. Chem.* **1990**, *29*, 1271–1285.
(42) Reisner, E.; Arion, V. A.; Guedes da Silva, M. F. C.; Lichtenecker, R.; Eichinger, A.; Keppler, B. K.; Kukushkin, V. Yu.; Pombeiro, A. J. L. *Inorg. Chem.* **2004**, *43*, 7083–7093.
(43) Bacac, M.; Hotze, A. C. G.; van der Schilden, K.; Haasnoot, J. G.; Pacor, S.; Alessio, E.; Sava, G.; Reedijk, J. *J. Inorg. Biochem.* **2004**, *98*, 402–412.
(44) Kapitza, S.; Pongratz, M.; Jakupec, M. A.; Heffeter, P.; Berger, W.; Lackinger, L.; Keppler, B. K.; Marian, B. *J. Cancer. Res. Clin. Oncol.* **2005**, *131*, 101–110.

Table 5. Cytotoxicity of Six Osmium(IV) Complexes in Three Human Cancer Cell Lines

	IC_{50} (μM)[a]		
compound	CH1	A549	SW480
6	26 ± 6	77 ± 20	18 ± 3
7	73 ± 24	247 ± 29	114 ± 5
8	160 ± 55	453 ± 15	391 ± 16
9	142 ± 20	229 ± 27	105 ± 3
10	148 ± 75	329 ± 126	163 ± 60
11	151 ± 28	434 ± 10	322 ± 79

[a] 50% inhibitory concentrations (means ± standard deviation), as obtained by the MTT assay (continuous exposure for 96 h).

osmium(IV) compound **10** is markedly less cytotoxic despite the lower charge of the complex anion, adding another facet to the hard to predict activity relationships of related ruthenium and osmium compounds.

Final Remarks. Controlled exploration of Anderson type rearrangement reactions of $(H_2azole)_2[Os^{IV}Cl_6]$ in dry ethanol or in isoamyl alcohol in the presence of tetrabutylammonium chloride enabled the synthesis of complexes of the general formula $[cation]^+[Os^{IV}Cl_5(Hazole)]^-$, where $[cation]^+ = n\text{-}Bu_4N^+$, Hazole = 1*H*-pyrazole, 1*H*-indazole, 1*H*-imidazole, 1*H*-benzimidazole, or 1*H*,2,4-triazole. The efficacy of the observed transformation appears to be dependent on the electron-donating potency of the azole heterocycle and the solvent used. A deeper substitution at osmium(IV) with formation of *trans*-$[Os^{IV}Cl_4(Hazole)_2]$ complexes was observed in the case of imidazole and benzimidazole systems with the most pronounced electron-donating properties and highest basicity. Comparison of the osmium complexes described in this work with related ruthenium analogues, namely, $(H_2azole)_2[Ru^{III}Cl_5(Hazole)]$[9,12,45] and $(H_2azole)[Ru^{III}Cl_4(Hazole)_2]$,[12,46] shows a clear preference for higher oxidation states of the heavier congener. Preparation of better water-soluble analogues of the $[Os^{IV}Cl_5(Hazole)]^-$ compounds in the form of sodium and azolium salts permitted the assessment of their antiproliferative activity in vitro against human cancer cell lines. The results reported herein provide an entry to the chemistry of *trans*-bis(azole)tetrachloridoosmium(IV) complexes. Investigations directed at the synthesis and characterization of this type of compounds are underway in our laboratory. This work is of particular interest if one takes into account that the related ruthenium analogue $(H_2ind)[Ru^{III}Cl_4(Hind)_2]$ is a potent anticancer drug in clinical trials. In addition, a notable crystallographic contribution has been made. The compounds **1**−**6** are the first complexes of the type $[Os^{IV}Cl_5(Hazole)]^-$, and **12** is the first *trans*-$[Os^{IV}Cl_4(Hazole)_2]$ complex characterized by X-ray crystallography.

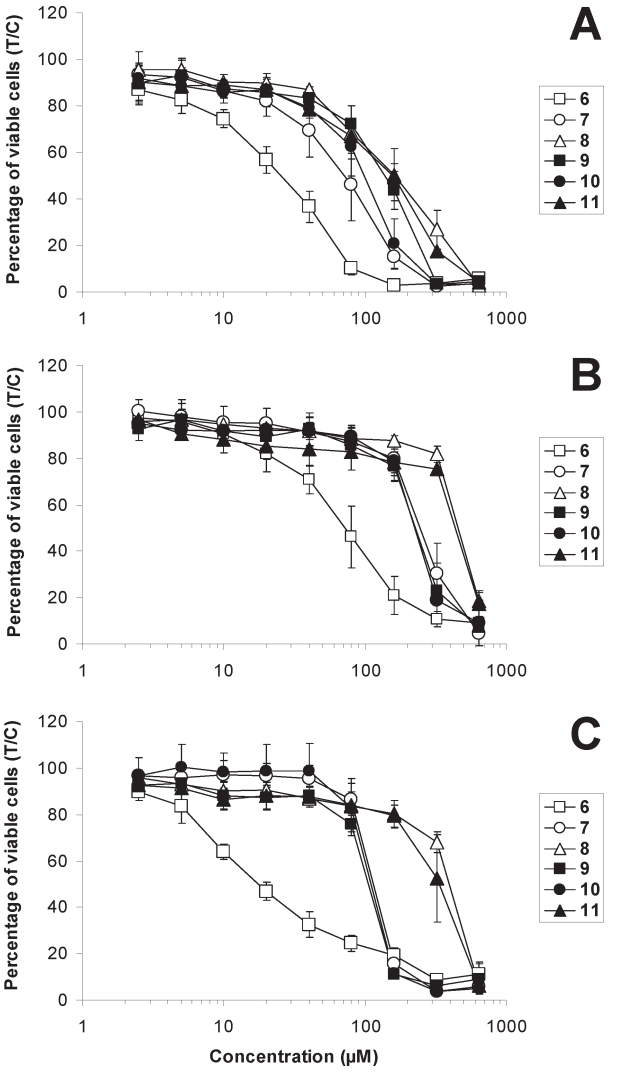

Figure 11. Concentration-effect curves of six osmium(IV) complexes in the human cancer cell lines CH1 (A), A549 (B), and SW480 (C), as obtained by the MTT assay (continuous exposure for 96 h).

Acknowledgment. We thank Anatoly Dobrov for the measurement of ESI mass spectra, Alexander Roller for the collection of X-ray data, Lukas Filak for cyclic voltammetry measurements, and Prof. Dr. Markus Galanski for 2D NMR measurements. We are also indebted to Prof. Dr. Liviu Chibotaru for motivating discussions.

Supporting Information Available: Synthesis of $(H_2trz)_2[OsCl_6]$, UV−vis spectra of **6** and **7** in water and of **1**, **2**, **4**, **5**, and **12** in ethanol, $^{13}C,^1H$ HSQC spectra of **1**, **2** and **9**, $^{15}N,^1H$ HSQC spectra of **1**, **2** and **9**, $^{13}C,^1H$ HMBC spectra of **2** and **9**, $^1H,^1H$ NOESY and $^1H,^1H$ COSY spectra of **2**, cyclic voltamogramms of **2**, **4** and **5** in DMSO, magnetic data for **5**, X-ray crystallographic files in CIF format for **1**−**6** and **12**. This material is available free of charge via the Internet at http://pubs.acs.org.

(45) Smith, C. A.; Sutherland-Smith, A. J.; Kratz, F.; Baker, E. N.; Keppler, B. H. *J. Biol. Inorg. Chem.* **1996**, *1*, 424–431.
(46) Hartinger, C. G.; Zorbas-Seifried, S.; Jakupec, M. A.; Kynast, B.; Zorbas, H.; Keppler, B. K. *J. Inorg. Biochem.* **2006**, *100*, 891–904.